

Cubic C₂₀: An intrinsic superconducting carbon allotrope

Ying Yu,¹ Xun-Wang Yan,² Fengjie Ma,³ Miao Gao,^{1,4,*} and Zhong-Yi Lu⁵

¹Department of Physics, School of Physical Science and Technology, Ningbo University, Zhejiang 315211, China

²College of Physics and Engineering, Qufu Normal University, Shandong 273165, China

³The Center for Advanced Quantum Studies and Department of Physics, Beijing Normal University, Beijing 100875, China

⁴School of Physics, Zhejiang University, Hangzhou 310058, China

⁵Department of Physics, Renmin University of China, Beijing 100872, China

(Dated: January 31, 2023)

Finding new phases of carbon is an interesting topic. Based on density functional first-principles calculations, we propose the first cubic metallic carbon allotrope, namely sc-C₂₀. The elastic properties, electronic structure, lattice dynamics, and phonon-mediated superconductivity of sc-C₂₀ are systematically studied. It is found that the metallicity originates from the p orbitals of carbon atoms, which are perpendicular to the sp^2 -bonding planes. The electron-phonon coupling is accurately computed with Wannier interpolation method. By solving the isotropic Eliashberg equations self-consistently, we predict that sc-C₂₀ is an intrinsic carbon superconductor, without introducing any guest atoms or doping, whose transition temperature is determined to be 24.6 K. Moreover, the formation energy of sc-C₂₀ is lower than those of body-centered-cubic C₈ and T-carbon which have been synthesized. In combination with the dynamical stability ascertained by phonon spectrum, we believe there is a high probability to obtain sc-C₂₀ in experiment.

I. INTRODUCTION

The studies of carbon-based superconductor can be traced back to the 1960s. Superconductivity was first discovered in graphite intercalation compounds (GICs) below 1 K, such as KC₈ [1]. Metastable GICs with higher metal concentration were synthesized under high pressure, with the superconducting transition temperature (T_c) being slightly boosted to 1.9 K in LiC₂ [2] and 5 K in NaC₂ [3]. Under ambient pressure, the highest T_c for GICs was 11.5 K in CaC₆ [4]. Graphene, the two-dimensional form of graphite, has gapless Dirac bands. Superconductivity in doped graphene has been extensively investigated [5–8]. Recently, correlated insulating states were observed in twisted bilayer graphene, and superconductivity emerges at 1.7 K after electrostatic doping [9, 10]. For twisted trilayer graphene, rich phase diagram and better tunability of electric field were realized, compared with the bilayer case [11, 12], providing a fascinating playground to explore the interplay between correlated states and superconductivity. Insulator to superconductor transition was reported in boron-doped diamond [13], in which the T_c exhibits a positive dependence on the proportion of boron that incorporated into diamond [14]. It was reported that the onset T_c of 27% boron-doped Q-carbon is 55 K [15]. Fullerene shows superconductivity at 18 K, after the potassium intercalation with stoichiometry of K₃C₆₀ [16]. Subsequently, the T_c was improved to 33 K in RbCs₂C₆₀ [17] and 40 K in Cs₃C₆₀ [18]. Signatures of superconductivity were also detected in single- and multi-walled carbon nanotubes [19, 20]. However, the superconductivity transition is quite sensitive to the configuration of Au electrode [20]. Organic compounds are important components of carbon-based superconductors, for example, (TMTSF)₂PF₆ [21], (BEDT-TTF)₂X [22], and K_{3,3}Picene [23].

As what mentioned above, introducing guest atom or doping is inescapable to realize superconductivity in carbon materials. Therefore, it is quite interesting to know whether there is a carbon allotrope showing intrinsic superconductivity. To achieve this purpose, the first step is finding metallic carbon allotropes, which has drawn lots of attentions for decades. Since pure sp^3 -hybridization always leads to insulating state for carbon, like diamond, including sp^2 -bonded carbon atoms is a general strategy to realize metallicity. Hoffman *et al.* proposed a metallic body-centered tetragonal carbon in 1983, namely bct-4 [24, 25], which consists of zigzag carbon chains bonded along the c axis. Similar to bct-4, H-6 carbon, another three-dimensional sp^2 network, was suggested [26]. However, H-6 carbon is unstable, which can continuously transform to diamond without destroying any bonds [27, 28]. The bulk modulus of a face-centered cubic carbon was investigated [29], called fcc-C₂₀ hereafter. But this structure can not maintain its dynamical stability [30]. Mathematical analysis showed that perfect sp^2 hybridization is compatible with the cubic symmetry, resulting in a K_4 crystal [31]. Although K_4 carbon is a metal [32, 33], substantial imaginary modes emerge in its phonon spectrum, which can be rationalized in terms of the absence of π bonding [34]. Utilizing orthogonal nanoribbons of graphene and biphenylene [35], metallic GT-8 and GT-12 carbon were constructed [36]. Besides these sp^2 carbon allotropes, several metallic carbon materials were proposed with sp^2 - sp^3 hybridized bonding configurations, for example, T6-carbon [37], Hex-C₂₄ [38], Hex-C₁₈ [39], H₁₈ carbon [40], C14-diamond [41], O-type carbon and T-type carbon [42]. In addition, a fully sp^3 -hybridized metallic carbon, called Tri-C₉, built through distorting the sp^3 bonds, was suggested [43]. However, the electron-phonon coupling (EPC) and potential phonon-mediated superconductivity in these metallic carbon allotropes have never been investigated so far. Very recently, different structural models were adopted to study the superconductivity of graphite-diamond hybrid, with predicted T_c ranging from 2 K to 42 K [44]. Thus, the phase space of superconducting carbon allotrope needs to be

* gaomiao@nbu.edu.cn

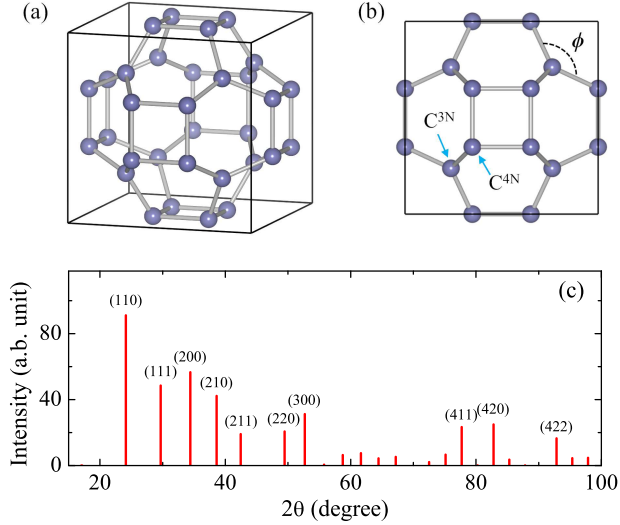


FIG. 1. (a) Three-dimensional view of the ball-stick model of sc-C₂₀. (b) View along the [001] direction. The solid black lines represent the cubic unit cell. (c) The simulated XRD pattern of sc-C₂₀. The Miller indices are labelled aside the diffraction main peaks. In our simulation, the X-ray wavelength is adopted as 1.5418 Å.

further enriched.

In this work, we design a simple cubic crystal of carbon, called sc-C₂₀. Based on the first-principles calculations, the atomic structure, elastic properties, X-ray diffraction pattern, electronic structure, phonons, and superconductivity of sc-C₂₀ are investigated. As revealed by our calculations, sc-C₂₀ inherently possesses metallicity. Phonon modes, including A_{2u} , T_{2g} , A_{1g} , E_g , and A_{2g} , involve in the EPC, providing multiple channels to pair electrons. Through Wannier interpolation, the EPC constant λ and ω_{log} are equal to 0.63 and 60.81 meV, respectively, giving rise to superconductivity with T_c being 24.6 K. As a comparison, the EPC and T_c are also determined for several metallic carbons proposed before, including Hex-C₂₄, bct-4, C14-diamond, T6, and H₁₈ carbon. None of these compounds show superconductivity above 8 K.

II. RESULTS AND DISCUSSIONS

The crystal structure of sc-C₂₀ is shown in Fig. 1. Carbon atoms can be classified into two types. Eight sp^2 -bonded carbon atoms are seated close to the cell corners. Twelve sp^3 -hybridized carbon atoms locate around the face centers of the cubic cell, forming squares. According to the number of the nearest neighbors, these two nonequivalent carbon atoms are denoted as C^{3N} and C^{4N}, respectively [Fig. 1(b)]. sc-C₂₀ belongs to the space group $Pm\bar{3}m$ (No. 221). After optimization, the lattice constant of sc-C₂₀ is found to be 5.2135 Å. C^{3N} and C^{4N} occupy 8g (0.2376, 0.2376, 0.2376) and 12i (0.0000, 0.3485, 0.3485) Wyckoff positions. The bond angle ϕ is 119.9° [Fig. 1(b)], indicating a perfect sp^2 hybridization, like in graphene. The mechanical stability of

sc-C₂₀ is examined by calculating the elastic constants C_{ij} . For cubic crystals, there are only three independent C_{ij} coefficients, namely C_{11} , C_{12} , and C_{44} , which are determined to be 537.0 GPa, 224.2 GPa, and 228.1 GPa, respectively. It is known that the mechanical stability conditions for cubic systems are $C_{11} - C_{12} > 0$, $C_{11} + 2C_{12} > 0$, and $C_{44} > 0$ [45], which are satisfied by sc-C₂₀. Using Voigt-Reuss-Hill approximation [46], the bulk modulus B , shear modulus G , Young modulus E , and Poisson's ratio ν are found to be 328.5 GPa, 196.1 GPa, 490.7 GPa, and 0.25, respectively. We also estimate the Vickers hardness of sc-C₂₀ with Chen's model [47], $H_v = 2(k^2 G)^{0.585} - 3$, in which the Pugh modulus ratio $k = G/B$. As a result, sc-C₂₀ is not a superhard material with H_v of 21.0 GPa. The simulated X-ray diffraction (XRD) pattern is presented in Fig. 1 (c), which can be used to check the sign of its existence in experiment.

Figure 2 shows the energy-volume relation for twelve carbon allotropes. By setting the total energy of equilibrium sc-C₂₀ to zero, the lowest energies for diamond, C14-diamond, Hex-C₂₄, H₁₈, bct-4, T6-carbon, bcc-C₈, fcc-C₂₀, H-6, K₄, and T-carbon are -46.32, -38.72, -36.93, -20.99, -20.41, -12.80, 0.04, 7.87, 11.65, 39.89, and 40.91 meV/atom. Among the metallic carbons, the energy of sc-C₂₀ lies in the middle. In particular, sc-C₂₀ is energetically favorable with respect to fcc-C₂₀, H-6, and K₄. Interestingly, sc-C₂₀ is more stable compared with two synthesized insulating carbons, i.e., bcc-C₈ [48] and T-carbon [49–51]. This indicates that the synthesis of sc-C₂₀ in experiment is feasible. At the equilibrium structure, the density ρ of sc-C₂₀ is 2.81 g/cm³, in comparison with 3.52 g/cm³ in diamond and 1.50 g/cm³ in T-carbon [51].

The electronic structure of sc-C₂₀ is presented in Fig. 3. It is clear that sc-C₂₀ is a metal, with two energy bands across the Fermi level [Fig. 3(a)]. Since PBE functional always underestimates the band gap, we also calculate the band structure using the hybrid functional HSE06 [52, 53]. Although, a repulsion effect is observed in comparison with the PBE bands. The

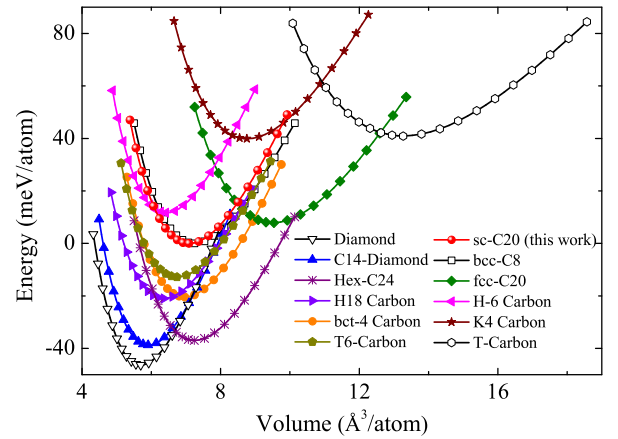


FIG. 2. Total energies versus volume for various carbon allotropes. The total energy of fully relaxed sc-C₂₀ is set to zero. The datum of insulating carbons are presented by black color and hollow symbols.

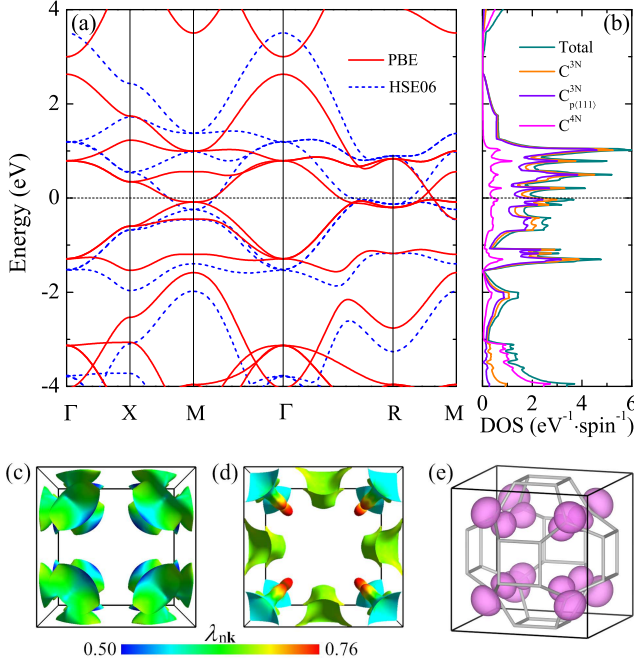


FIG. 3. Electronic structure for sc-C₂₀. (a) Band structure. The Fermi level is set to zero. The solid red and blue dotted lines represent the energy bands generated with PBE and HSE06 functionals, respectively. (b) Total and partial density of states. (c)-(d) Distribution of \mathbf{k} -resolved EPC constant $\lambda_{\mathbf{nk}}$ on the Fermi surfaces. (e) Isosurface of charge density of strongly coupled electronic Kohn-Sham states. The isovalue is chosen to be 0.025 e/Bohr^3 . Here, state at \mathbf{k} point (0.26, 0.26, 0.26) on the Fermi surface, together with its equivalent ones are taken into consideration.

HSE06 results resemble those of the PBE around the Fermi level. According to the partial density of states (DOS), C^{3N} atoms dominate the DOS from -3.0 eV to 3.0 eV [Fig. 3(b)]. Specifically, they contribute about 81.5% of the DOS at the Fermi level, i.e. $N(0)$. The p orbitals of C^{3N} that perpendicular to the sp^2 -bonding plane are along the $\langle 111 \rangle$ direction, which are denoted as $C_{p(111)}^{3N}$. In particular, the DOS of C^{3N} almost originates from the $C_{p(111)}^{3N}$ orbitals. Nevertheless, contribution of C^{4N} atoms mainly lies below -3.0 eV. The Fermi surfaces are shown in Fig. 3(c) and Fig. 3(d), with color mapping of the EPC strength $\lambda_{\mathbf{nk}}$. All the pieces of the Fermi surfaces are close to the boundaries of Brillouin zone. The hotspots in Fig. 3(d) stand for the Kohn-Sham states that possess the strongest coupling with phonons. As confirmed by the charge distribution, these strongly coupled electronic states just correspond to the $C_{p(111)}^{3N}$ orbitals [Fig. 3(e)].

Figure 4 shows the phonon spectrum and phonon DOS. Beside mechanical stability, sc-C₂₀ is proved to be dynamically stable, as indicated by the phonon spectrum, whereas no imaginary phonon modes appear [Fig. 4(a)]. The symmetries of phonon modes which strongly couple with electrons are marked. For instance, the A_{2u} mode at X point, T_{2g} , A_{1g} , E_g , and A_{2g} modes at Γ point. The highest peak of phonon DOS is around 150 meV, originating from dispersionless modes [Fig.

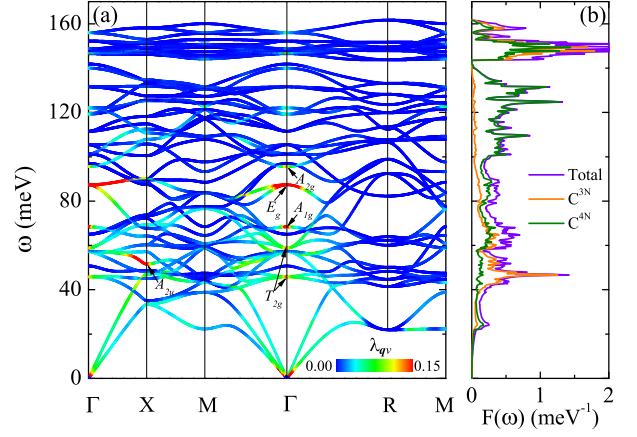


FIG. 4. Lattice dynamics of sc-C₂₀. (a) Phonon spectrum, colored by EPC constant $\lambda_{\mathbf{qv}}$. (b) Total and projected phonon DOS $F(\omega)$.

4(b)]. These modes mix the movements of C^{4N} and C^{3N} atoms together, as demonstrated by the projected phonon DOS. The vibration of C^{4N} holds a dominant position from 80 meV to 140 meV. The situation is reversed below 60 meV. To date, carbon allotropes that either synthesized or predicted with cubic symmetry, including diamond, bcc-C₈, T-carbon, cubic graphene [54, 55], Y-carbon and TY-carbon [56], are all insulating. Although, the unit cells of fcc-C₂₀ and K₄ are cubic, they are dynamically unstable. This makes sc-C₂₀ the first cubic metallic carbon maintaining dynamical stability.

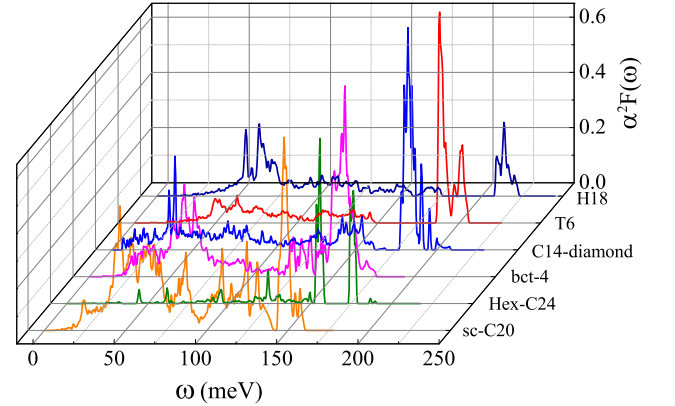


FIG. 5. Eliashberg spectral function $\alpha^2 F(\omega)$ for sc-C₂₀. As a comparison, the calculated results of Hex-C₂₄, bct-4, C14-diamond, T6, and H₁₈ carbon allotropes are also shown. For these compounds, fine electron \mathbf{k} grids of $48 \times 48 \times 48$, $90 \times 90 \times 30$, $12 \times 72 \times 72$, $72 \times 72 \times 36$, and $30 \times 30 \times 90$ points are employed. The phonon \mathbf{q} meshes are divided into $16 \times 16 \times 16$, $30 \times 30 \times 10$, $4 \times 24 \times 24$, $24 \times 24 \times 12$, and $10 \times 10 \times 30$ points. Such ultradense samplings of the Brillouin zone ensure the convergence of EPC constant λ .

The Eliashberg spectral functions $\alpha^2 F(\omega)$ of several metal-

lic carbon allotropes are given in Fig. 5. The multi-peak behavior of $\alpha^2F(\omega)$ in sc-C₂₀ naturally reflects the existences of various strongly coupled phonon modes uncovered in Fig. 4 (a). The peak near 150 meV is beneficial from the large phonon DOS. In contrast, the reduced peak around 87 meV can be attributed to the limited DOS, although the E_g modes at Γ point have sizeable EPC strength. By comparing with other carbon allotropes, such as Hex-C₂₄, bct-4, C14-diamond, T6, and H₁₈, two important features of $\alpha^2F(\omega)$ are revealed for sc-C₂₀. On one hand, the phonons of sc-C₂₀ exhibit significant softening, with the highest phonon frequency being about 160 meV, which is compressed by 27.4% with respect to that in H₁₈ carbon. On the other hand, $\alpha^2F(\omega)$ in sc-C₂₀ overwhelms those of Hex-C₂₄, bct-4, C14-diamond, T6, and H₁₈ carbons in the intermediate frequency range, for example, from 80 meV to 120 meV. These two factors play vital roles in the enhancement of EPC in sc-C₂₀. Owing $\alpha^2F(\omega)$ in hand, the EPC constant λ and logarithmic average frequency ω_{\log} can be acquired through $\lambda = 2 \int \frac{\alpha^2F(\omega)}{\omega} d\omega$, and $\omega_{\log} = \exp \left[\frac{2}{\lambda} \int \frac{d\omega}{\omega} \alpha^2F(\omega) \ln \omega \right]$. We find that the EPC constants λ are 0.63, 0.07, 0.42, 0.37, 0.16, 0.21 in sc-C₂₀, Hex-C₂₄, bct-4, C14-diamond, T6, and H₁₈, respectively. The logarithmic average frequencies ω_{\log} are computed to be 60.81, 111.60, 66.28, 47.10, 88.23, and 72.18 meV, correspondingly.

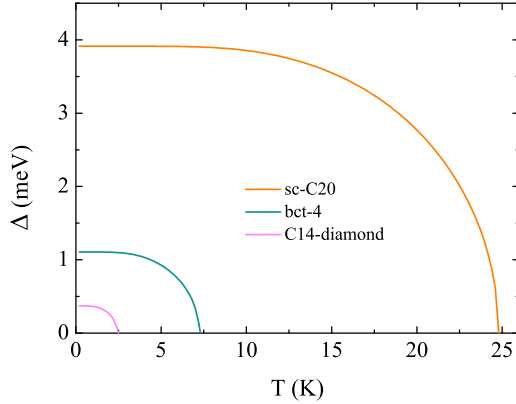


FIG. 6. Superconducting energy gaps versus temperature for sc-C₂₀, bct-4, and C14-diamond.

Firstly, we estimate the T_c by the McMillan-Allen-Dynes formula [57]. As a consequence, the T_c is 18.8 K in sc-C₂₀, 4.2 K in bct-4, and 1.3 K in C14-diamond. No superconducting transition occurs in Hex-C₂₄, T6, and H₁₈ carbons. In order to determine the T_c more accurately, the isotropic Eliashberg equations are solved [58, 59]. In our calculations, the screened Coulomb potential μ^* is set to 0.1. Finally, the transition tem-

peratures are calculated to be 24.6 K, 7.2 K, and 2.4 K, for sc-C₂₀, bct-4, and C14-diamond [Fig. 6]. At low temperature, the superconducting energy gaps are equal to 3.91, 1.11, and 0.37 meV, respectively. Our findings strongly suggest that sc-C₂₀ is a unique intrinsic superconducting carbon allotrope, with T_c even higher than most carbon-based superconductors.

III. CONCLUSION

In summary, a cubic carbon allotrope is constructed, which is not only a metal, but also a superconductor with sizeable T_c . There is no need to introduce guest atoms or doping to realize superconductivity, unlike other carbon-based compounds. This makes sc-C₂₀ a fascinating intrinsic carbon superconductor. The unpaired p orbitals that pointing to the corners of the cubic cell can account for the metallicity. The symmetries of strongly coupled phonon modes are identified.

ACKNOWLEDGMENTS

This work was supported by the National Natural Science Foundation of China (Grant Nos. 11974194, 11974207, 12074040, 11934020, and 11888101). M.G. was also sponsored by K. C. Wong Magna Fund in Ningbo University.

Appendix A: Calculation Methods

Our density functional theory calculations were carried out based on the plane wave basis and pseudopotential methods. The Quantum-ESPRESSO package was adopted [60]. We calculated the electronic states and phonon perturbation potentials [61] using the generalized gradient approximation (GGA) of Perdew-Burke-Ernzerhoff formula [62] and the optimized norm-conserving Vanderbilt pseudopotentials [63]. The kinetic energy cut-off and the charge density cut-off were set to 80 Ry and 320 Ry, respectively. A \mathbf{k} mesh of $18 \times 18 \times 18$ points in combination with a Methfessel-Paxton smearing [64] of 0.02 Ry, was employed to calculate the self-consistent charge densities. Within the framework of density-functional perturbation theory [65], we computed the dynamical matrices and the perturbation potentials on a $6 \times 6 \times 6$ mesh. To construct the maximally localized Wannier functions of sc-C₂₀ [66], we chose 36 hybridized σ states localized in the middle of carbon-carbon bonds and 8 s -type functions at the sp^2 -bonded carbon sites. The convergence of EPC constant λ was extensively checked through fine electron ($60 \times 60 \times 60$) and phonon ($20 \times 20 \times 20$) grids with the Electron-Phonon Wannier codes [67]. The Dirac δ -functions for electrons and phonons were smeared out by a Gaussian function with the widths of 30 meV and 0.5 meV, respectively. We determined the T_c by solving the isotropic Eliashberg equations. The sum over Matsubara frequencies was truncated with $\omega_c = 16$ eV, about 100 times that of the highest phonon frequency.

[1] N. B. Hannay, T. H. Geballe, B. T. Matthias, K. Andres, P. Schmidt, and D. MacNair, *Phys. Rev. Lett.* **14**, 225 (1965).

[2] I. T. Belash, A. D. Bronnikov, O. V. Zharikov, and A. V. Pal'nichenko, *Solid State Commun.* **69**, 921 (1989).

- [3] I. T. Belash, A. D. Bronnikov, O. V. Zharikov, and A. V. Pal'nichenko, *Synth. Met.* **36**, 283 (1990).
- [4] N. Emery, C. Hérold, M. d'Astuto, V. Garcia, Ch. Bellin, J. F. Marêché, P. Lagrange, and G. Loupiau, *Phys. Rev. Lett.* **95**, 087003 (2005).
- [5] B. Uchoa and A. H. Castro Neto, *Phys. Rev. Lett.* **98**, 146801 (2007).
- [6] G. Profeta, M. Calandra, and F. Mauri, *Nat. Phys.* **8**, 131 (2012).
- [7] C. Si, Z. Liu, W. Duan, and F. Liu, *Phys. Rev. Lett.* **111**, 196802 (2013).
- [8] J. Chapman, Y. Su, C. A. Howard, D. Kundys, A. N. Grigorenko, F. Guinea, A. K. Geim, I. V. Grigorieva, and R. R. Nair, *Sci. Rep.* **6**, 23254 (2016).
- [9] Y. Cao, V. Fatemi, A. Demir, S. Fang, S. L. Tomarken, J. Y. Luo, J. D. Sanchez-Yamagishi, K. Watanabe, T. Taniguchi, E. Kaxiras, R. C. Ashoori, and P. Jarillo-Herrero, *Nature* **556**, 80 (2018).
- [10] Y. Cao, V. Fatemi, S. Fang, K. Watanabe, T. Taniguchi, E. Kaxiras, and P. Jarillo-Herrero, *Nature* **556**, 43 (2018).
- [11] Z. Zhu, S. Carr, D. Massatt, M. Luskin, and E. Kaxiras, *Phys. Rev. Lett.* **125**, 116404 (2020).
- [12] J. M. Park, Y. Cao, K. Watanabe, T. Taniguchi, and P. Jarillo-Herrero, *Nature* **590**, 249 (2021).
- [13] E. A. Ekimov, V. A. Sidorov, E. D. Bauer, N. N. Mel'nik, N. J. Curro, J. D. Thompson, and S. M. Stishov, *Nature* **428**, 542 (2004).
- [14] Y. Takano, T. Takenouchi, S. Ishii, S. Ueda, T. Okutsu, I. Sakaguchi, H. Umezawa, H. Kawarada, and M. Tachiki, *Diamond Relat. Mater.* **16**, 911 (2007).
- [15] A. Bhaumik, R. Sachan, S. Gupta, and J. Narayan, *ACS Nano* **11**, 11915 (2017).
- [16] A. F. Hebard, M. J. Rosseinsky, R. C. Haddon, D. W. Murphy, S. H. Glarum, T. T. M. Palstra, A. P. Ramirez, and A. R. Kortan, *Nature* **350**, 600 (1991).
- [17] K. Tanigaki, T. W. Ebbesen, S. Saito, J. Mizuki, J. S. Tsai, Y. Kubo, and S. Kuroshima, *Nature* **352**, 222 (1991).
- [18] T. T. M. Palstra, O. Zhou, Y. Iwasa, P. E. Sulewski, R. M. Fleming, and B. R. Zegarski, *Solid State Commun.* **93**, 327 (1995).
- [19] M. Kociak, A. Yu. Kasumov, S. Guéron, B. Reulet, I. I. Khodos, Yu. B. Gorbatov, V. T. Volkov, L. Vaccarini, and H. Bouchiat, *Phys. Rev. Lett.* **86**, 2416 (2001).
- [20] I. Takesue, J. Haruyama, N. Kobayashi, S. Chiashi, S. Maruyama, T. Sugai, and H. Shinohara, *Phys. Rev. Lett.* **96**, 057001 (2006).
- [21] D. Jérôme, A. Mazaud, M. Ribault, and K. Bechgaard, *J. de Phys. Lett.* **41**, 95 (1980).
- [22] A. M. Kini, U. Geiser, H. H. Wang, K. D. Carlson, J. M. Williams, W. K. Kwok, K. G. Vandervoort, J. E. Thompson, D. L. Stupka, D. Jung, and M.-H. Whangbo, *Inorg. Chem. Commun.* **29**, 2555 (1990).
- [23] R. Mitsuhashi, Y. Suzuki, Y. Yamanari, H. Mitamura, T. Kambe, N. Ikeda, H. Okamoto, A. Fujiwara, M. Yamaji, N. Kawasaki, Y. Maniwa, and Y. Kubozono, *Nature* **464**, 76 (2010).
- [24] R. Hoffman, T. Hughbanks, M. Kertesz, and P. H. Bird, *J. Am. Chem. Soc.* **105**, 4831 (1983).
- [25] A. Y. Liu and M. L. Cohen, *Phys. Rev. B* **45**, 4579 (1992).
- [26] M. A. Tamor and K. C. Hass, *J. Mater. Res.* **5**, 2273 (1990).
- [27] A. Y. Liu, M. L. Cohen, K. C. Hass, and M. A. Tamor, *Phys. Rev. B* **43**, 6742 (1991).
- [28] Z. G. Fthenakis, *RSC Adv.* **6**, 78187 (2016).
- [29] M. Côté, J. C. Grossman, M. L. Cohen, and S. G. Louie, *Phys. Rev. B* **58**, 664 (1998).
- [30] We have calculated the phonon spectrum of fcc-C₂₀, in which lots of imaginary modes appear.
- [31] T. Sunada, *Not. Am. Math. Soc.* **55**, 208 (2008).
- [32] G.-M. Rignanese and J.-C. Charlier, *Phys. Rev. B* **78**, 125415 (2008).
- [33] M. Itoh, M. Kotani, H. Naito, T. Sunada, Y. Kawazoe, and T. Adachi, *Phys. Rev. Lett.* **102**, 055703 (2009).
- [34] Y. Yao, J. S. Tse, J. Sun, D. D. Klug, R. Martoňák, and T. Iitaka, *Phys. Rev. Lett.* **102**, 229601 (2009).
- [35] Q. Fan, L. Yan, M. W. Tripp, Ondřej Krejčí, S. Dimosthenous, S. R. Kachel, M. Chen, A. S. Foster, U. Koert, P. Liljeroth, and J. M. Gottfried, *Science* **372**, 852 (2021).
- [36] M. Hu, X. Dong, B. Yang, B. Xu, D. Yu and J. He, *Phys. Chem. Chem. Phys.* **17**, 13028 (2015).
- [37] S. Zhang, Q. Wang, X. Chen, and P. Jena, *Proc. Natl. Acad. Sci. USA* **110**, 18809 (2013).
- [38] H. Bu, M. Zhao, W. Dong, S. Lu, and X. Wang, *J. Mater. Chem. C* **2**, 2751 (2014).
- [39] J. Liu, T. Zhao, S. Zhang, and Q. Wang, *Nano Energy* **38**, 263, (2017).
- [40] C.-X. Zhao, C.-Y. Niu, Z.-J. Qin, X. Ren, J.-T. Wang, J. Cho, and Y. Jia, *Sci. Rep.* **6**, 21879 (2016).
- [41] X. Wu, X. Shi, M. Yao, S. Liu, X. Yang, L. Zhu, T. Cui, and B. Liu, *Carbon* **123**, 311 (2017).
- [42] Y. Liu, X. Jiang, J. Fu, and J. Zhao, *Carbon* **126**, 601 (2018).
- [43] Y. Cheng, R. Melnik, Y. Kawazoe, B. Wen, *Cryst. Growth Des.* **16**, 1360 (2016).
- [44] Y. Ge, K. Luo, Y. Liu, G. Yang, W. Hu, B. Li, G. Gao, X.-F. Zhou, B. Xu, Z. Zhao, and Y. Tian, *Mater. Today Phys.* **23**, 100630 (2022).
- [45] M. Born and K. Huang, *Am. J. Phys.* **23**, 474 (1955).
- [46] R. Hill, *Proc. Phys. Soc. A* **65**, 349 (1952).
- [47] X.-Q. Chen, H. Y. Niu, D. Z. Li, and Y. Y. Li, *Intermetallics* **19**, 1275 (2011).
- [48] P. Liu, H. Cui, and G. W. Yang, *Cryst. Growth Des.* **8**, 581 (2008).
- [49] J. Zhang, R. Wang, X. Zhu, A. Pan, C. Han, X. Li, D. Zhao, C. Ma, W. Wang, H. Su, and C. Niu, *Nat. Commun.* **8**, 683 (2017).
- [50] K. Xu, H. Liu, Y.-C. Shi, J.-Y. You, X.-Y. Ma, H.-J. Cui, Q.-B. Yan, G.-C. Chen, and G. Su, *Carbon* **157** 270 (2020).
- [51] X.-L. Sheng, Q.-B. Yan, F. Ye, Q.-R. Zheng, and G. Su, *Phys. Rev. Lett.* **106**, 155703 (2011).
- [52] J. Heyd, G. E. Scuseria, and M. Ernzerhof, *J. Chem. Phys.* **118**, 8207 (2003).
- [53] J. Heyd, G. E. Scuseria, and M. Ernzerhof, *J. Chem. Phys.* **124**, 219906 (2006).
- [54] M. O'Keeffe, G. B. Adams, and O. F. Sankey, *Phys. Rev. Lett.* **68**, 2325 (1992).
- [55] X. Shen, D. M. Ho, and R. A. Pascal, *J. Am. Chem. Soc.* **126**, 5798 (2004).
- [56] J. Y. Jo and B. G. Kim, *Phys. Rev. B* **86**, 075151 (2012).
- [57] P. B. Allen and R. C. Dynes, *Phys. Rev. B* **12**, 905 (1975).
- [58] G. M. Eliashberg, *Sov. Phys. JETP* **11**, 696 (1960).
- [59] E. R. Margine and F. Giustino, *Phys. Rev. B* **87**, 024505 (2013).
- [60] P. Giannozzi *et al.*, *J. Phys.:Condens. Matter* **21**, 395502 (2009).
- [61] F. Giustino, M. L. Cohen, and S. G. Louie, *Phys. Rev. B* **76**, 165108 (2007).
- [62] J. P. Perdew, K. Burke, and M. Ernzerhof, *Phys. Rev. Lett.* **77**, 3865 (1996).
- [63] D. R. Hamann, *Phys. Rev. B* **88**, 085117 (2013).
- [64] M. Methfessel and A. T. Paxton, *Phys. Rev. B* **40**, 3616 (1989).
- [65] S. Baroni, S. de Gironcoli, A. Dal Corso, and P. Giannozzi, *Rev. Mod. Phys.* **73**, 515 (2001).

- [66] G. Pizzi *et al.*, [J. Phys.: Condens. Matter](#) **32**, 165902 (2020).
- [67] S. Ponc , E. R. Margine, C. Verdi, and F. Giustino, [Comp. Phys. Commun.](#) **209**, 116 (2016).